Journal of Biomolecular NMR **29:** 139–150, 2004.

Characterization of threonine side chain dynamics in an antifreeze protein using natural abundance ^{13}C NMR spectroscopy

Margaret E. Daley & Brian D. Sykes*
Department of Biochemistry, CIHR Group in Protein Structure and Function and Protein Engineering Network of Centres of Excellence, University of Alberta, Edmonton, Alberta T6G 2H7, Canada

Received 6 August 2003; Accepted 17 December 2003

Key words: antifreeze protein, natural abundance ^{13}C NMR, side chain dynamics

Abstract

The dynamics of threonine side chains of the *Tenebrio molitor* antifreeze protein (TmAFP) were investigated using natural abundance ^{13}C NMR. In TmAFP, the array of threonine residues on one face of the protein is responsible for conferring its ability to bind crystalline ice and inhibit its growth. Heteronuclear longitudinal and transverse relaxation rates and the $\{^1H\}$-^{13}C NOE were determined in this study. The CαH relaxation measurements were compared to the previously measured ^{15}N backbone parameters and these are found to be in agreement. For the analysis of the threonine side chain motions, the model of restricted rotational diffusion about the χ_1 dihedral angle was employed [London and Avitabile (1978) *J. Am. Chem. Soc.*, **100**, 7159–7165]. We demonstrate that the motion experienced by the ice binding threonine side chains is highly restricted, with an approximate upper limit of less than $\pm 25°$.

Abbreviations: AFP, antifreeze protein; HSQC, heteronuclear single quantum coherence; NMR, nuclear magnetic resonance; NOE, nuclear Overhauser effect; R_1, longitudinal relaxation rate; R_2, transverse relaxation rate.

Introduction

The study of protein dynamics is of fundamental importance towards a complete understanding of their biological function. Nuclear magnetic resonance (NMR) spectroscopy is widely used to examine the internal motions of proteins over a range of time-scales, including large amplitude slow motions (seconds), intermediate and exchange motions (milli- to microseconds), and fast bond vector fluctuations (nano- to picoseconds) all of which are significant in various biological contexts (Kay, 1998). The heteronuclear NMR relaxation techniques most often employed are sensitive to these subnanosecond internal motions. With increasing evidence that picosecond protein dynamics may be relevant to the retention of entropy in protein-ligand binding (Kay et al., 1998), measurements of this type will further contribute to a full description of the relationship between protein structure and function.

The widespread use of ^{15}N NMR relaxation measurements has provided a great deal of information on protein backbone dynamics, however a complete description requires information about side chain motions as well. For this, the use of ^{13}C spectroscopy is necessary. Side chain dynamics have been examined by various methods, both on proteins that are uniformly ^{13}C/^{15}N labeled (Yamazaki et al., 1994; Engelke and Rüterjans, 1998) or those that are partially labeled by either random fractional ^{13}C labeling (Wand et al., 1996) or the incorporation of ^{13}C into alternating carbon positions (LeMaster and Kushlan, 1996), both of which avoid complicated data interpretation arising from the large ^{13}C-^{13}C scalar and dipolar couplings. The incorporation of deuterium as a spin relaxation probe at various side chain positions (Muhandiram et al., 1995; Yang et al., 1998) has also proven extremely valuable.

*To whom correspondence should be addressed. E-mail: brian.sykes@ualberta.ca

In the absence of ^{13}C labeling, the use of natural abundance ^{13}C NMR spectroscopy has allowed the examination of protein motions despite sensitivity limitations (Nirmala and Wagner, 1988; Dellwo and Wand, 1989; Palmer et al., 1991a; Mispelter et al., 1995). While many natural abundance ^{13}C NMR experiments have been successful, the techniques are best suited for methine carbon relaxation because the simpler system allows for greater ease of analysis. Methylene and methyl carbon relaxation by natural abundance methods is considerably more complex owing to cross-correlation effects (Sklenar et al., 1987; Kay and Torchia, 1991; Palmer et al., 1991b). These techniques have not only enabled study of the motions of backbone Cα and side chain methine carbons, but have also permitted direct comparison to backbone ^{15}N measurements (Guenneugues et al., 1999). In the case of the ^{15}N nucleus, relaxation occurs through both the dipolar interaction with its attached amide proton and its chemical shift anisotropy, while for natural abundance ^{13}C, relaxation of aliphatic carbons is dominated only by the dipole-dipole interaction with the directly attached proton. The advantage of focusing on these nearly ideal two-spin systems is that the heteronuclear relaxation is attributed to the reorientation of the HX bond vector with respect to the direction of the magnetic field and can be analyzed in terms of the local motions being superimposed on the overall protein tumbling. However, the choice of an appropriate model for the motion is often difficult and internal motion can be interpreted either using model-free approaches (Lipari and Szabo, 1982a,b; Clore et al., 1990a,b) or in terms of specific motional models including wobbling-in-a-cone (Lipari and Szabo, 1980, 1981), site jump, or restricted diffusion models (London, 1980).

For the antifreeze protein from the beetle *Tenebrio molitor* (TmAFP), we have previously completed a full analysis of ^{15}N backbone relaxation parameters at both 30 °C and 5 °C (Daley et al., 2002). These studies showed that TmAFP is a well-folded and rigid β-helical protein with restricted internal mobility throughout the backbone. Owing to difficulties in the expression and purification of this highly disulfide-bonded protein (Liou et al., 2000), we have not been able to obtain ^{13}C labeled TmAFP. In order to study side chain motions in this protein, and in particular, the threonine side chains which comprise the ice-binding face (Marshall et al., 2002), we have chosen to investigate the dynamics of the χ_1 dihedral angles connecting the β-CH of threonine to its corresponding α-CH. In our previous study of TmAFP side chains (Daley and Sykes, 2003), we analyzed the internal dynamics of the threonine χ_1 angles using motionally averaged $^3J_{\alpha\beta}$ ^1H-^1H scalar coupling constants. Using the Karplus relations (Karplus 1959, 1963) and the relative intensities of the intraresidue NOEs involving the Hα and Hβ protons (Clore and Gronenborn, 1989), populations of the staggered rotamer conformations are calculated by fitting the $^3J_{\alpha\beta}$ coupling constant to the measured value. We observed that threonine residues on the ice-binding face preferentially maintain a $\chi_1 = -60°$ rotamer conformation and concluded that a rigid preformed ice binding structure is adopted in solution prior to ice surface recognition. However, using averaged J coupling constants provides no information about the rates of transfer between rotameric states or of librational motions. In this paper, we examine the χ_1 dihedral angle dynamics using ^{13}C methine relaxation rates measured at natural abundance.

Experimental procedures

NMR spectroscopy

Methine ^{13}C relaxation experiments were performed on a single previously prepared sample of TmAFP isoform 2-14 at natural ^{13}C abundance. The lyophilized protein was dissolved in 100% D_2O, with 0.1 mM DSS added for internal referencing. The final protein concentration was approximately 2 mM and the pH was adjusted to 5.6 with microliter aliquots of 100 mM NaOD or DCl as required. No evidence of dimerization in solution has been observed in any NMR measurements of TmAFP and sedimentation ultracentrifugation has confirmed the monomeric state of the protein in solution up to this concentration (Liou et al., 2000). The NMR experiments were performed using Varian INOVA 500 MHz and Unity 600 MHz spectrometers equipped with 5 mm triple resonance probes and z-axis pulsed field gradients. ^{13}C-R_1, -R_2, and $\{^1H\}$-^{13}C NOE experiments were carried out at 125.7 and 150.8 MHz at both 30 °C and 5 °C using sensitivity-enhanced gradient HSQC pulse sequences adapted from those of Farrow et al. (1994). The CH/CH_3 – edited HSQC spectrum of TmAFP is displayed in Figure 1 with assignments of CαH and CβH resonances labeled.

The spectral widths for ^1H and ^{13}C for the R_1 and NOE experiments at each temperature were 5500.0

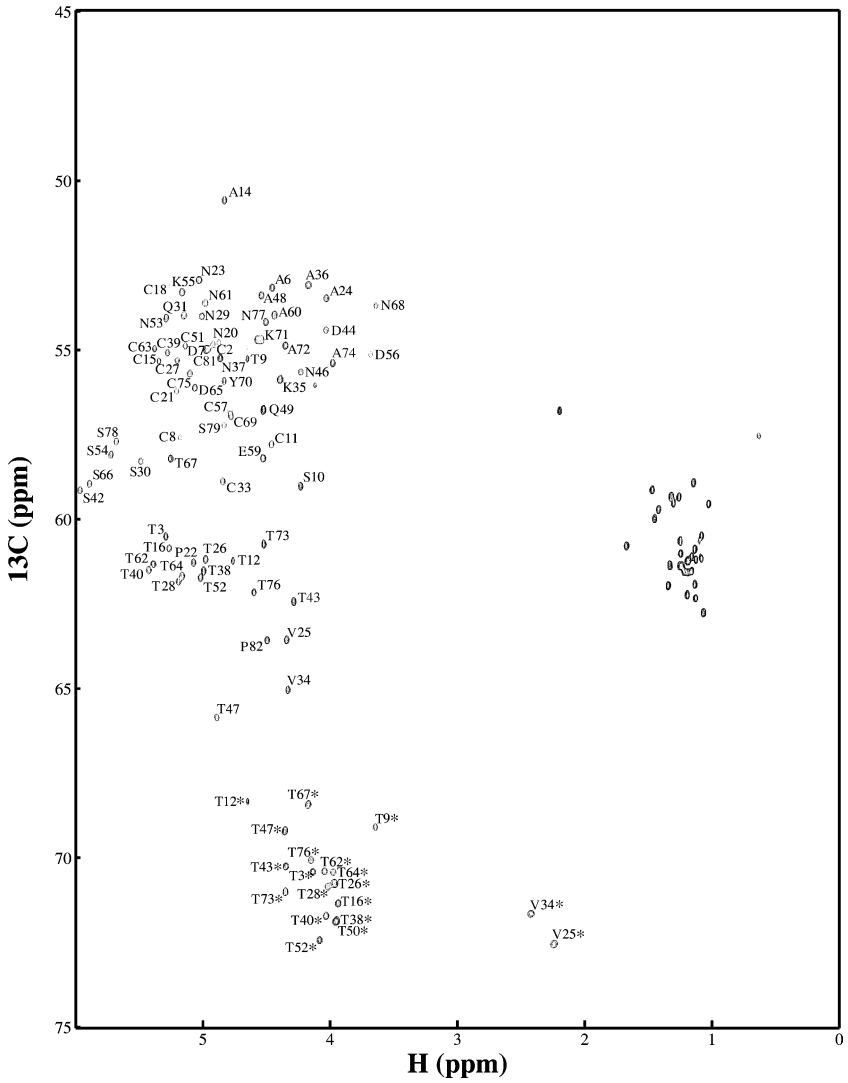

Figure 1. ^{1}H-^{13}C HSQC correlation spectrum of TmAFP methine and methyl resonances. The labels display the assignment of the CαH and CβH correlations. The asterisks differentiate the CβH correlations from the CαH correlations of the same residue.

and 5000.0 Hz at 500 MHz, and 6400.0 and 6000.0 Hz at 600 MHz, respectively. The ^{1}H carrier was set at the residual HDO resonance, and the ^{13}C carrier was set at 56.7 ppm. The number of complex points acquired for ^{1}H and ^{13}C, respectively, were 396 and 128 (R_1), 396 and 160 (R_2), or 396 and 48 (NOE) at 500 MHz, and 436 and 128 (R_1), 410 and 96 (R_2), or 410 and 48 (NOE) at 600 MHz. A total of 48 (at 500 MHz) or 64 (at 600 MHz) transients were collected for ^{13}C-R_1. At 500 and 600 MHz, 256 transients were accumulated for the measurement of {^{1}H}-^{13}C NOE. For the measurement of ^{13}C-R_2 at 30 °C, reduced spectral widths of 2837.081 Hz at 500 MHz and 3404.57 Hz at 600 MHz were used in the F_1 (^{13}C) dimension and the ^{13}C carrier was moved to 62.7 ppm to minimize off-resonance effects on the relaxation of the Cβ resonances.

For measurement of ^{13}C-R_1 relaxation rates, delays of 10.1, 50.5, 111.1, 181.8, 252.5, 353.5, 454.5, and 606.1 ms were used at both 500 and 600 MHz. At 5 °C, delays of 10.1, 50.7, 111.5, 182.5, 253.5, 354.9, 456.3, and 608.4 ms were used. Measurement of ^{13}C-R_2 relaxation rates, at 30 °C only, employed delays of 16.3, 32.6, 48.9, 65.2, 81.5, 97.8, 114.1, and 130.4 ms at both 500 and 600 MHz. In order to obtain equilibrium, a 2.0 s delay between repetitions of the pulse sequence for ^{13}C-R_1 measurements was employed,

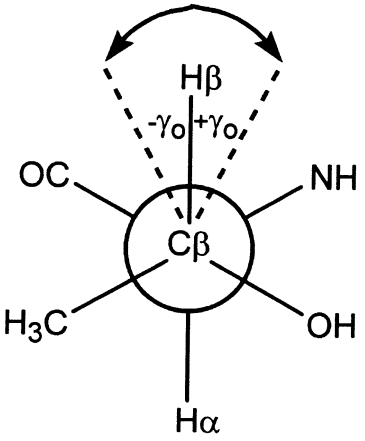

Figure 2. Restricted rotation of $\pm\,\gamma_0$ around the Cα-Cβ bond. The threonine side chain is displayed as a Newman projection with the Cα in the back and the Cβ in the front. Rotation about the χ_1 angle is perpendicular to the plane of the page.

while the delay for obtaining equilibrium during the measurement of ^{13}C-R_2 was 5 s in order to minimize sample heating. Within the CPMG sequence, the delay between ^{13}C 180° pulses was 900 μs. The ^{13}C 180° pulse width was 121 μs, while the ^{1}H 180° pulse width was 16 μs. {^{1}H}-^{13}C steady-state NOEs were measured from two HSQC spectra acquired with and without proton saturation prior to the first ^{13}C excitation pulse. For the experiment with ^{1}H saturation, a relaxation delay of 2 s followed by proton saturation using a train of 120° proton pulses with 5 ms pulse intervals for 3 s prior to the first ^{13}C pulse was employed. For the spectra with no ^{1}H saturation, a delay of 5 s between repetitions of the pulse sequence was used.

NMR data processing

All NMR data were processed with the NMRPipe software (Delaglio et al., 1995). Enhanced sensitivity data were processed using the ranceY.M macro. The F_1 (^{13}C) dimension was extended by 64 complex points using linear prediction before zero filling. The F_2 (^{1}H) dimension was multiplied by a 60°-shifted sine-bell function and the F_1 dimension was multiplied by a 60°-shifted squared sine-bell function before Fourier transformation. The F_1 and F_2 dimensions were baseline corrected by polynomial subtraction in the frequency domain. The NMRView program (Johnson and Blevins, 1994) was used for peak picking of all ^{13}C-HSQC spectra. The values of the peak intensities for the ^{13}C-R_1 and -R_2 measurements were fit to single-exponential, two-parameter decay curves using the available NMRView rate analysis scripts. The range of errors in the precision of the ^{13}C-R_1 and -R_2 fits were obtained from non-linear least-squares fits of the peak intensities to two-parameter exponential decays and varied between 3–6% at 30°C. However, we have estimated the accuracy of the measurements to be less (∼10%) based on the signal-to-noise ratio of the natural abundance data at low concentrations. Error in the {^{1}H}-^{13}C NOE values was calculated from baseplane noise values in ^{13}C-HSQC spectra acquired with and without proton saturation.

Table 1. Threonine and valine ^{13}C-R_1 measurements at 600 MHz and 30 °C

Residue	Cα R_1 (s^{-1})	Cβ R_1 (s^{-1})	$R_{1\alpha}/R_{1\beta}$
Thr 3	1.41 ± 0.14	2.21 ± 0.22	0.64
Thr 9	1.56 ± 0.16	1.44 ± 0.14	1.09
Thr 12	1.38 ± 0.14	1.53 ± 0.15	0.90
Thr 16	1.37 ± 0.14	1.45 ± 0.14	0.94
Val 25	1.53 ± 0.15	2.20 ± 0.22	0.69
Thr 26	1.62 ± 0.16	1.65 ± 0.16	0.98
Thr 28	1.53 ± 0.15	1.53 ± 0.15	1.00
Val 34	1.28 ± 0.13	2.09 ± 0.21	0.61
Thr 40	1.34 ± 0.13	1.49 ± 0.15	0.90
Thr 47	1.23 ± 0.12	2.20 ± 0.22	0.56
Thr 52	1.60 ± 0.16	1.67 ± 0.17	0.96
Thr 62	1.34 ± 0.13	1.27 ± 0.13	1.06
Thr 64	1.20 ± 0.12	1.45 ± 0.14	0.83
Thr 67	1.55 ± 0.16	1.80 ± 0.18	0.86
Thr 73	1.30 ± 0.13	1.61 ± 0.16	0.81
Average	1.42	1.71	0.86
St. Dev.	0.14	0.32	0.16

Theory

The choice of the theoretical model that best fits the measured relaxation parameters can be difficult, especially with a limited amount of data; in general the simplest model that adequately describes the measured parameters should be used. In this paper, we decided not to use the model-free approach for the analysis, but instead have chosen to interpret the relaxation data using the rotational restricted diffusion model (London and Avitabile, 1978), which allows coverage of a broad range of amplitudes and time scales around the χ_1 dihedral angle (Engelke and Ruterjans, 1998).

Table 2. Threonine ^{13}C-R_2 measurements at 600 MHz and 30 °C

Residue	Cα R_2 (s^{-1})	Cβ R_2 (s^{-1})	$R_{2\alpha}/R_{2\beta}$
Thr 3	26.10 ± 2.6	17.55 ± 1.8	1.49
Thr 9	16.73 ± 1.7	23.88 ± 2.4	0.70
Thr 16	19.39 ± 1.9	21.97 ± 2.2	0.88
Thr 28	17.43 ± 1.7	16.27 ± 1.6	1.07
Thr 47	19.99 ± 2.0	12.05 ± 1.2	1.66
Thr 52	23.74 ± 2.4	14.61 ± 1.5	1.63
Thr 62	26.84 ± 2.7	33.82 ± 3.4	0.79
Thr 64	19.45 ± 1.9	15.46 ± 1.5	1.26
Thr 67	18.04 ± 1.8	13.18 ± 1.3	1.37
Thr 73	26.70 ± 2.7	21.05 ± 2.1	1.27
Thr 76	25.28 ± 2.5	18.63 ± 1.9	1.36
Average	22.11	17.89	1.35
St. Dev.	3.81	6.29	0.44

Table 3. Threonine and valine NOE measurements at 600 MHz and 30 °C

Residue	Cα NOE	Cβ NOE	NOEα/NOEβ
Thr 3	1.35 ± 0.06	1.07 ± 0.05	1.26
Thr 9	1.28 ± 0.07	1.30 ± 0.06	0.98
Thr 12	1.28 ± 0.09	1.33 ± 0.13	0.96
Val 25	1.50 ± 0.06	1.34 ± 0.05	1.12
Val 34	1.24 ± 0.05	1.35 ± 0.07	0.92
Thr 40	1.31 ± 0.06	1.30 ± 0.08	1.01
Thr 47	1.13 ± 0.07	1.52 ± 0.05	0.74
Thr 62	1.13 ± 0.06	1.25 ± 0.09	0.90
Thr 67	1.09 ± 0.05	1.19 ± 0.05	0.92
Thr 73	1.03 ± 0.04	0.86 ± 0.06	1.19
Average	1.23	1.25	1.00
St. Dev.	0.14	0.18	0.15

This model allows for free internal diffusion over a restricted range subject to boundary conditions that limit the range of motion. Specifically, the ^{13}Cβ-^{1}Hβ bond vector moves around χ_1 with an amplitude in the range $-\gamma_0 \leq \gamma \leq \gamma_0$ (Figure 2).

To fully examine the internal motion of the χ_1 dihedral angle, ^{13}C-R_1 and R_2 relaxation rates and the steady-state {^{1}H}-^{13}C NOE of the CH nuclei were measured. As mentioned briefly in the introduction, ^{13}C methine relaxation is caused by the dipolar interaction with its directly attached proton and the chemical shift anisotropy and cross-correlation between these two effects can safely be neglected in the simulations performed (Wittebort and Szabo, 1978). In the experiments measured, the pulse sequences employed eliminate cross-correlation by the application of ^{1}H 180° pulses as mentioned in the Experimental Procedures. The expressions for the relaxation rate constants ^{13}C-R_1 and R_2 and the heteronuclear NOE are given by (Abragam, 1961):

$$R_1 = \frac{\left(\frac{h}{2\pi}\right)^2 \gamma_H^2 \gamma_C^2}{4r_{CH}^6} [J(\omega_H - \omega_C) + 3J(\omega_C) + 6J(\omega_H + \omega_C)] \quad (1)$$

$$R_2 = \frac{\left(\frac{h}{2\pi}\right)^2 \gamma_H^2 \gamma_C^2}{8r_{CH}^6} [4J(0) + J(\omega_H - \omega_C) + 3J(\omega_C) + 6J(\omega_H) + 6J(\omega_H + \omega_C)] \quad (2)$$

$$\text{NOE} = 1 + \frac{\gamma_H [6J(\omega_H + \omega_C) - J(\omega_H - \omega_C)]}{\gamma_C [J(\omega_H - \omega_C) + 3J(\omega_C) + 6J(\omega_H + \omega_C)]} \quad (3)$$

where γ_H, γ_C and ω_H, ω_C correspond to the gyromagnetic ratios and Larmor frequencies of hydrogen and carbon, respectively, h is Planck's constant and r_{CH} is the C-H bond length (1.10 Å).

For the restricted diffusion motion about χ_1 in the range $\pm\ \gamma_0$, the correlation function is given by (London and Avitabile, 1978):

$$C(t) = \frac{1}{4\pi} e^{-6Dt} \sum_{m=-2}^{2} \sum_{n=0}^{\infty} a_m \left(E_{m,n}(\gamma_0)\right)^2 e^{\frac{-D_1 n^2 \pi^2 t}{(4\gamma_0)}}, \quad (4)$$

where $D_1 = 1/\tau_i$.

The corresponding spectral density function is the Fourier transform:

$$J(\omega) = \sum_{m=-2}^{2} \sum_{n=0}^{\infty} a_m \left(E_{m,n}(\gamma_0)\right)^2 \frac{2\tau_{cn}}{1 + (\omega\tau_{cn})^2}, \quad (5)$$

where $E_{m,n}(\gamma_0)$ is defined by:

$$\frac{\sin(m\gamma_0)}{m\gamma_0} \text{ for n=0}$$

$$\frac{1}{\sqrt{2}} \left(\frac{\sin\left(m\gamma_0 - n\frac{\pi}{2}\right)}{m\gamma_0 - n\frac{\pi}{2}} + (-1)^n \frac{\sin\left(m\gamma_0 + n\frac{\pi}{2}\right)}{m\gamma_0 + n\frac{\pi}{2}} \right) \quad (6)$$

for n ≠ 0

and

$$\tau_{cn} = \frac{4\gamma_0^2}{24D\gamma_0^2 + D_1 n^2 \pi^2}, \quad (7)$$

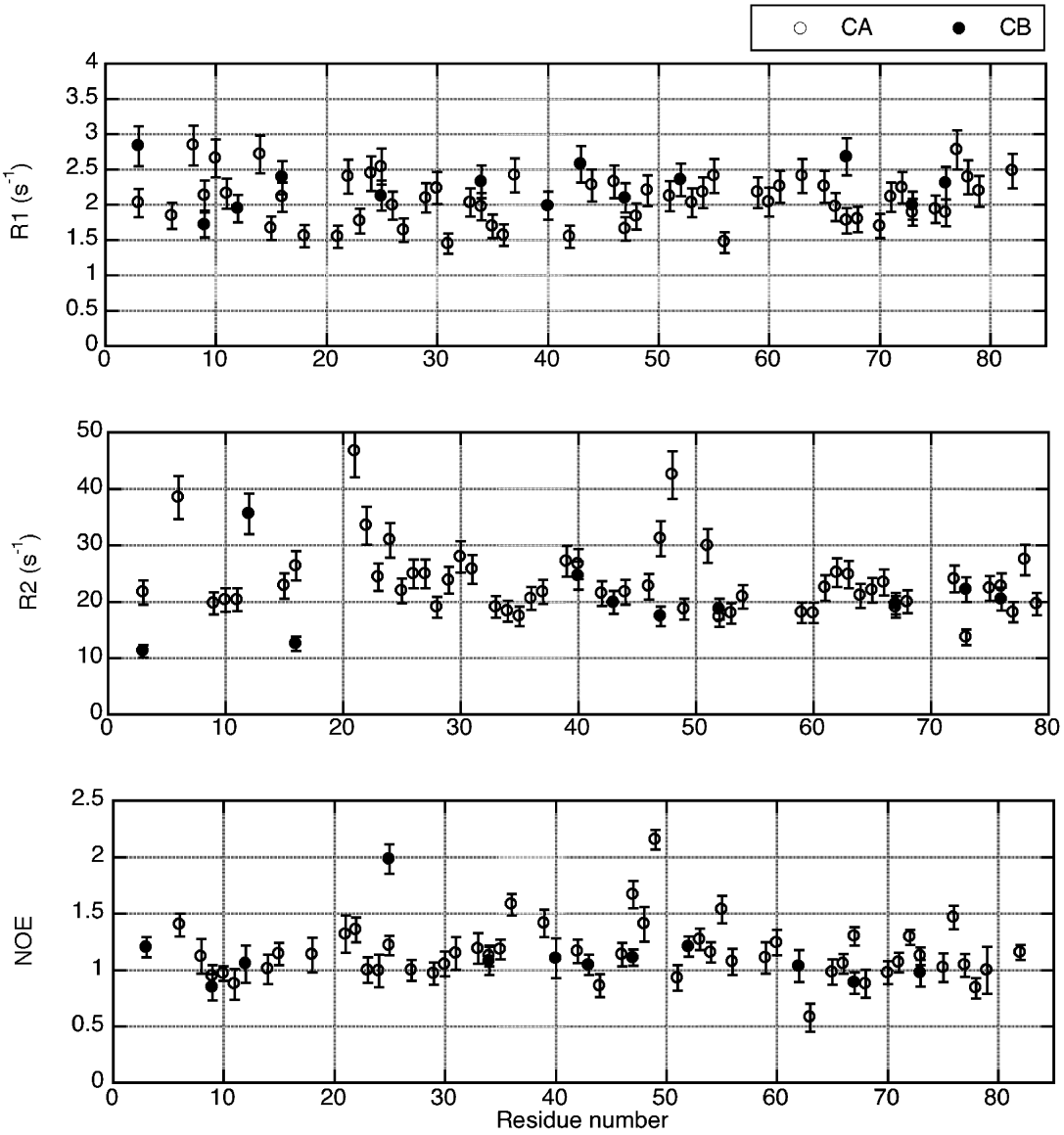

Figure 3. Plots of ^{13}C-R$_1$, ^{13}C-R$_2$, and {^{1}H}-^{13}C NOE at 500 MHz and 30 °C with individual error bars plotted for Cα (open circles) and Cβ (filled circles).

where $D = 1/6\tau_c$. The constants are given by $a_{\pm 2} = 0.2961$, $a_{\pm 1} = 0.1486$ and $a_0 = 0.1107$ (Engelke and Rüterjans, 1998).

London and Avitabile (1978) conclude for this model, that T_2 values provide a more useful interpretive tool for internal motion in most cases. They also state that T_1 and the NOE are valid only for diffusion coefficients where the free internal rotation calculation is in reasonable agreement with the $\gamma_0 = 180°$ calculation and when their behaviour with γ_0 is nearly monotonic, which criteria are satisfied for small proteins as used herein. Engelke and Rüterjans (1998) did not include T_2 values in the analysis of RNase T1 using this model, deriving qualitative lower limits for the amplitudes of motion from NOE values and including T_1 in the quantitative analysis to determine the upper limits for the internal correlation time. In the present paper, we will use both R_1 and R_2 relaxation rates as well as the NOE to estimate the amplitude of motion γ_0. The simulations were performed using the program Mathematica (Wolfram, 2002) using the

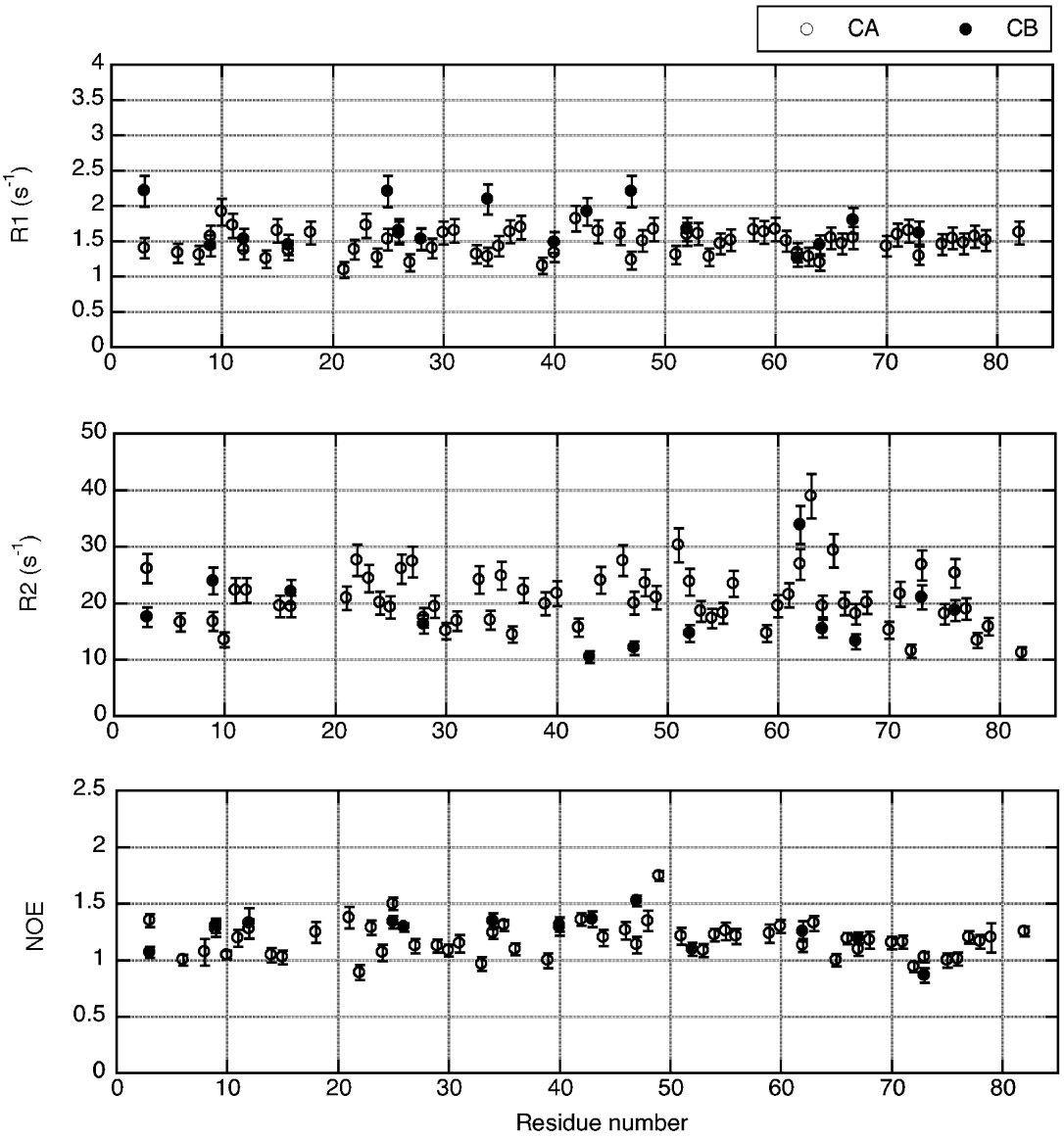

Figure 4. Plots of ^{13}C-R$_1$, ^{13}C-R$_2$, and {^{1}H}-^{13}C NOE at 600 MHz and 30 °C with individual error bars plotted for Cα (open circles) and Cβ (filled circles).

equations described and the parameters detailed in the following sections.

Results

$^{13}C - R_1, -R_2$, and NOE data

^{13}C methine relaxation parameters for TmAFP were studied at two temperatures, 30 and 5 °C. At 30 °C, the high resolution of the spectra allowed for 53–60 of 74 non-glycine Cα and 12–15 of 19 Cβ measurements at 600 MHz. Ranges for the number of resonances measured are given because of variability in peak overlap between the experiments at a given temperature and field. At 500 MHz, 50–54 Cα and 10-13 Cβ resonances were used in the analysis. The values of ^{13}C-R$_1$, -R$_2$ and NOE at 30 °C as a function of residue number are shown for the 500 MHz data in Figure 3 and the 600 MHz data in Figure 4. The ^{13}C-R$_1$, -R$_2$, and NOE measurements for the two resonance frequencies display similar profiles and restricted range of values. The R$_1$ values exhibit the characteristic magnetic field strength dependence, since for proteins in the slow

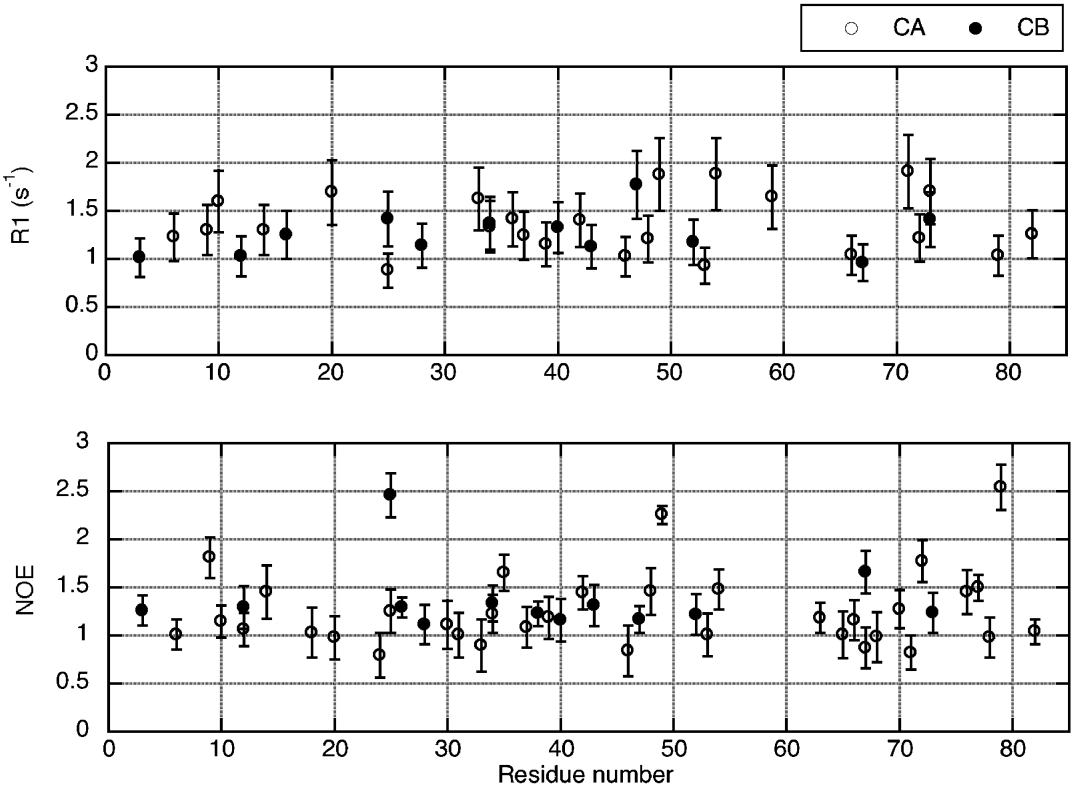

Figure 5. Plots of ^{13}C-R$_1$, and {^{1}H}-^{13}C NOE at 500 MHz and 5 °C with individual error bars plotted for Cα (open circles) and Cβ (filled circles).

tumbling limit, R_1 values are highly dependent on the rates of motion occurring at the Larmor frequency (Equation 1). The average $R_{1\alpha}^{500}$ over all Cα resonances is 2.07 ± 0.34 s^{-1}, and $R_{1\alpha}^{600}$ is 1.48 ± 0.17 s^{-1}. For the Cβ resonances, $R_{1\beta}^{500}$ is 2.26 ± 0.32 s^{-1} and $R_{1\beta}^{600}$ is 1.72 ± 0.31 s^{-1}. The R_2 values in the slow tumbling limit are dominated by the zero frequency value of the spectral density, J(0) (Equation 2), and are therefore similar at the different magnetic field strengths. The average $R_{2\alpha}^{500}$ is 23.4 ± 6.3 s^{-1} and $R_{2\alpha}^{600}$ is 20.7 ± 5.1 s^{-1}. For Cβ, the average $R_{2\beta}^{500}$ is 20.2 ± 6.7 s^{-1} and $R_{2\beta}^{600}$ is 18.2 ± 6.4 s^{-1}. The NOE values are highly sensitive to fast internal motion on the picosecond time-scale and the measurements are similar at the two field strengths. The average NOE_{α}^{500} is 1.15 ± 0.25 and NOE_{α}^{600} is 1.18 ± 0.15. For the Cβ resonances, NOE_{β}^{500} is 1.12 ± 0.29 and NOE_{β}^{600} is 1.25 ± 0.16.

The lower resolution of the spectra at 5 °C allowed for analysis of fewer resonances because of increased spectral overlap and the ^{13}C-R$_2$ values could not be obtained. At 600 MHz, 39-43 Cα and 10-13 Cβ could be measured, while at 500 MHz 24-35 Cα and 12-13 Cβ measurements were used. The values of ^{13}C-R$_1$ and the NOE at 5 °C are shown for the 500 MHz data in Figure 5 and the 600 MHz data in Figure 6. Again, at the two different resonance frequencies, the R_1 and NOE measurements display a similar profile and restricted range of values. The R_1 magnetic field strength dependence is obvious, where $R_{1\alpha}^{500}$ is 1.37 ± 0.30 s^{-1} and $R_{1\alpha}^{600}$ is 0.98 ± 0.36 s^{-1}. For the Cβ, $R_{1\beta}^{500}$ is 1.25 ± 0.23 s^{-1} and $R_{1\beta}^{600}$ is 1.02 ± 0.31 s^{-1}. The NOE measurements at 5 °C are quite similar to their measurements at 30 °C, with an average NOE_{α}^{500} of 1.25 ± 0.39 and NOE_{α}^{600} of 1.17 ± 0.21. The NOE_{β}^{500} is 1.36 ± 0.35, while NOE_{β}^{600} is 1.27 ± 0.31.

For the threonine and valine residues where both Cα and Cβ could be measured, the R_1, R_2, and NOE values of both resonances and their ratios (at 30 °C and 600 MHz) are displayed in Tables 1, 2 and 3, respectively.

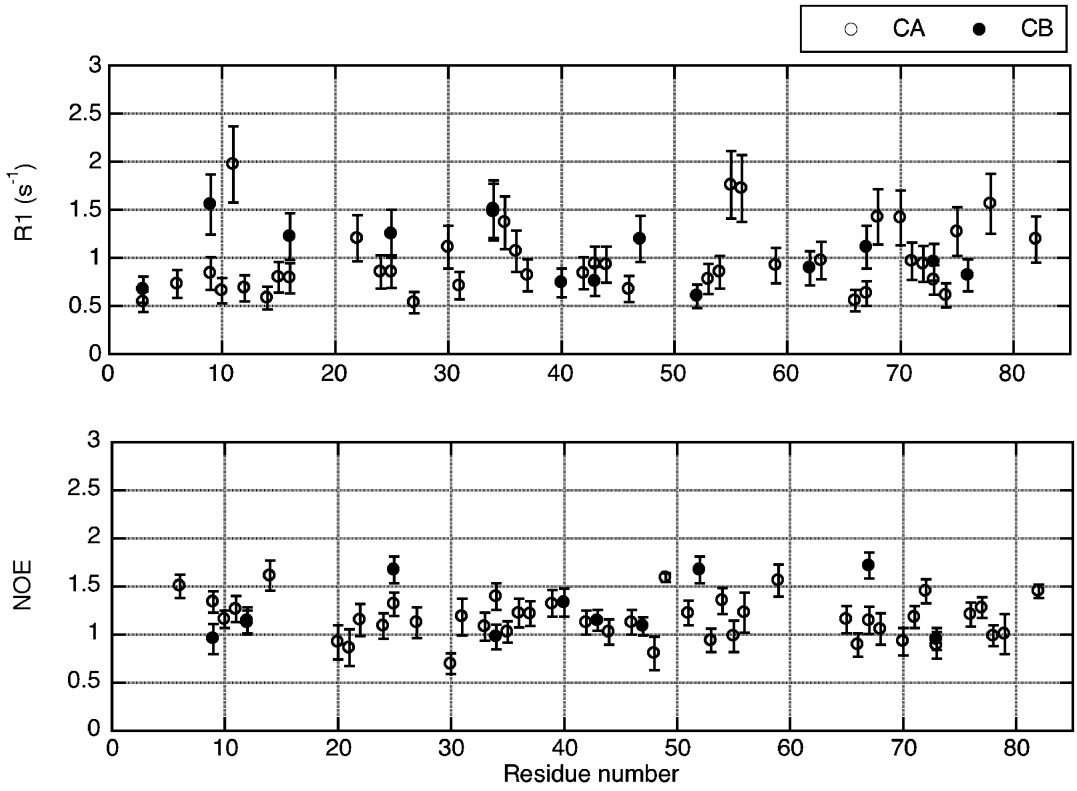

Figure 6. Plots of ^{13}C-R_1, and {^{1}H}-^{13}C NOE at 600 MHz and 5 °C with individual error bars plotted for Cα (open circles) and Cβ (filled circles).

Estimation of the overall correlation time

The overall rotational correlation time (τ_c) of TmAFP in D_2O was calculated with a grid search to find the minimum in the squared difference measured and calculated R_2/R_1 ratios of the Cα resonances using an in-house written program (Gagné et al., 1998). The calculation of τ_c was optimized using those residues that do not display obvious signs of relaxation active mobility using the criteria of Tjandra et al. (1995, 1996). The R_2/R_1 ratios of the selected residues should be dependent only on the global reorientation of the molecule, assuming negligible internal mobility and exchange. The global τ_c was then calculated on a per residue basis using the spectral density for isotropic rotational diffusion and the results averaged. A global τ_c of 4.5 ns at 600 MHz was obtained at 30 °C. This value is slightly higher than the τ_c of 4 ns obtained from the ^{15}N relaxation data (Daley et al., 2002), but is fully consistent with the increase in viscosity (η) of D_2O compared to H_2O. The value of η^{H2O} at 30 °C is 0.797 cP, while $\eta^{D2O} = 0.976$ cP (Cho et al., 1999), with a ratio of $\eta^{H2O}/\eta^{D2O} = 0.82$. The ratio $\tau_c^{H2O}/\tau_c^{D2O} = 0.89$, a value comparable to the ratio of the viscosities, indicating that the increase is attributable to the D_2O solution.

Discussion

In TmAFP we found that the τ_c^{D2O} calculated using the backbone CαH resonances was nearly equivalent to that measured previously from ^{15}N relaxation of NH vectors, allowing for the increased viscosity of D_2O. This indicates that the data from the two studies can be compared directly and that the CαH bond vectors are similarly rigid. Overall, it appears that the main chain CαH vectors behave in an analogous fashion to the restrictive motions of the backbone amide vectors. By comparing the average values of R_1, R_2 and NOE for the CαH to the CβH at 30 °C, it is clear that in general they are not significantly different and are within the error limits over the full length of the protein chain. In particular, for the threonine and valine residues that have both the CαH and CβH values measured from the same side chain, the calculated ratios shown in

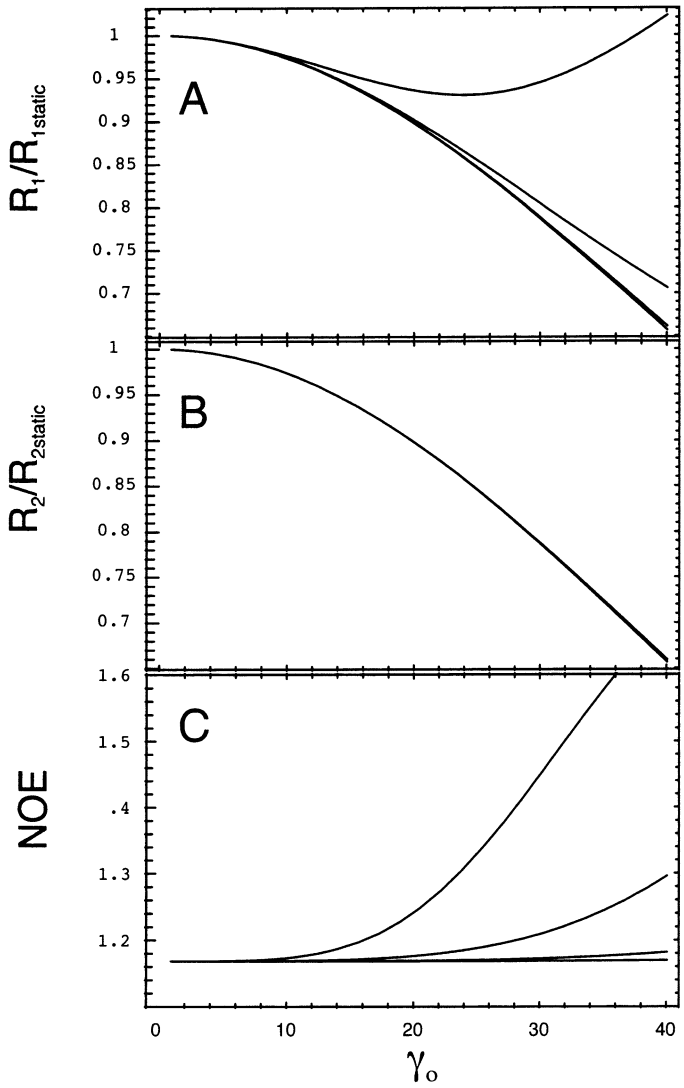

Figure 7. (A) Calculated graph of ^{13}C $R_1/R_{1static}$ vs γ_0 at four internal correlation times ($\tau_i = 10^{-9}$, 10^{-10}, 10^{-11}, and 10^{-12} s, from top to bottom), where $R_{1static}$ is the longitudinal relaxation rate in the absence of internal motion. (B) Calculated graph for ^{13}C $R_2/R_{2static}$ vs γ_0 at four internal correlation times ($\tau_i = 10^{-9}$, 10^{-10}, 10^{-11}, and 10^{-12} s, from bottom to top), where $R_{2static}$ is the transverse relaxation rate in the absence of internal motion. (C) Calculated graph of $\{^1$H$\}$-^{13}C NOE vs γ_0 at four internal correlation times ($\tau_i = 10^{-9}$, 10^{-10}, 10^{-11}, and 10^{-12} s, from top to bottom).

the tables indicate an overall restriction of motion for the CβH with respect to the CαH. Despite the fact that all of the threonine and valine side chains are presented on the surface of the protein, for most of the residues we do not observe increasing flexibility in the measurements towards the end of the side chain. It appears that for the threonine residues in TmAFP, the Cβ resonances are as rigid as the backbone and can be considered functionally as part of the backbone. The dominant restriction to this motion may be the favourable hydrogen bonding interactions that can be formed between the threonine side chain and the rigid backbone.

Theoretical plots for the R_1, R_2 and NOE as a function of γ_0 at various internal correlation times are shown in Figures 7A, B and C, respectively. These were calculated using the spectral density function in Equation 5, where τ_c is assumed to be 4.5 ns. Although from the ^{15}N relaxation data analysis we determined that TmAFP undergoes axially symmetric anisotropic rotation, here we do not include anisotropic overall reorientation in the calculations. All

calculations were performed using a τ_c of 4.5 ns, the 30 °C correlation time. At this temperature, the effects of axially symmetric rotation are not as pronounced as at 5 °C. However, the conclusions at 30 °C are also valid for the data at 5 °C, as on examination of the raw R_1 and NOE data presented in Figures 5 and 6, it is clear that the Cβ values are again in the same range as the Cα values. Therefore the discussion that follows can be extended to the data at both temperatures.

The results for $R_1/R_{1static}$, $R_2/R_{2static}$, and NOE as a function of γ_0 and corresponding to the values of D_0 and D_i specified are summarized in Figure 7. The values for each parameter are calculated out to $\gamma = 40°$. These results indicate that the relaxation parameters display very little dependence for smaller angles of displacement about the χ_1 angle. For the R_1, R_2 and NOE measurements of TmAFP, the values obtained indicate that the threonine side chains do not experience observable motions. By examination of the simulations in Figure 7, an upper limit for motion of γ_0 less than approximately 25° is assigned based on an estimate for error values of 10%.

Conclusions

Using a combination of experimental heteronuclear relaxation rates at ^{13}C natural abundance and rotational diffusion model calculations, we have demonstrated that the threonine side chains of the *Tenebrio molitor* antifreeze protein do not undergo significant motion about the χ_1 dihedral angle. This result agrees with our previous study of χ_1 angles by examination of $^3J_{\alpha\beta}$ coupling constants. In that study we observed that most of the threonine residues (including all of the ice-binding threonines) adopted specific rotameric conformations and did not experience a significant amount of rotameric averaging. Furthermore, by using heteronuclear relaxation measurements, we have identified that the restriction of motion occurs on the pico- to nanosecond time scale of bond vector and librational motions. It was not possible to make this conclusion on the basis of motionally averaged J couplings, which can arise from a combination of fast and slow time scale motions. The rigidity of the side chains in this small, β-helical protein is likely important for its ice binding activity, as it may reduce the entropic barrier for binding to a flat surface.

Acknowledgements

We thank Lewis Kay for pulse sequences, Matthew Crump and Leo Spyracopoulos for modifications to the pulse sequences, Gerry McQuaid for maintenance of the NMR spectrometers, and Peter Davies for the unlabeled TmAFP used in this study. This work is supported through grants from the Canadian Institutes of Health Research (CIHR) and Protein Engineering Network of Centres of Excellence. M.E.D. acknowledges CIHR for a Doctoral Research Award.

References

Abragam, A. (1961) *Principles of Nuclear Magnetism*, Clarendon Press, Oxford, U.K.

Cho, C.H., Urquidi, J., Singh, S. and Robinson, G.W. (1999) *J. Phys. Chem.*, **B103**, 1991–1994.

Clore, G.M. and Gronenborn, A.M. (1989) *Crit. Rev. Biochem. Mol. Biol.*, **24**, 479–557.

Clore, G.M., Driscoll, P.C., Wingfield, P.T. and Gronenborn, A.M. (1990a) *Biochemistry*, **29**, 7387–7401.

Clore, G.M., Szabo, A., Bax, A., Kay, L.E., Driscoll, P.C. and Gronenborn, A.M. (1990b) *J. Am. Chem. Soc.*, **112**, 4989–4991.

Daley, M.E. and Sykes, B.D. (2003) *Protein Sci.*, **12**, 1323–1331.

Daley, M.E., Spyracopoulos, L., Jia, Z., Davies, P.L. and Sykes, B.D. (2002) *Biochemistry*, **41**, 5515–5525.

Delaglio, F., Grzesiek, S., Vuister, G.W., Zhu, G., Pfeifer, J. and Bax, A. (1995) *J. Biomol. NMR*, **6**, 277–293.

Dellwo, M.J. and Wand, A.J. (1989) *J. Am. Chem. Soc.*, **111**, 4571–4578.

Engelke, J. and Rüterjans, H. (1998) *J. Biomol. NMR*, **11**, 165–183.

Farrow, N.A., Muhandiram, R., Singer, A.U., Pascal, S.M., Kay, C.M., Gish, G., Shoelson, S.E., Pawson, T., Forman-Kay, J.D. and Kay, L.E. (1994) *Biochemistry*, **33**, 5984–6003.

Gagné, S.M., Tsuda, S., Spyracopoulos, L., Kay, L.E. and Sykes, B.D. (1998) *J. Mol. Biol.*, **278**, 667–686.

Guenneugues, M., Gilquin, B., Wolff, N., Ménez, A. and Zinn-Justin, S. (1999) *J. Biomol. NMR*, **14**, 47–66.

Johnson, B.A. and Blevins, R.A. (1994) *J. Biomol. NMR*, **4**, 603–614.

Karplus, M. (1959) *J. Chem. Phys.*, **30**, 11–15.

Karplus, M. (1963) *J. Am. Chem. Soc.*, **85**, 2870–2871.

Kay, L.E. (1998) *Biochem. Cell Biol.*, **76**, 145–152.

Kay, L.E. and Torchia, D.A. (1991) *J. Magn. Reson.*, **95**, 536–547.

Kay, L.E., Muhandiram, R., Wolf, G., Shoelson, S.E. and Forman-Kay, J.D. (1998) *Nat. Struct. Biol.*, **5**, 156–163.

LeMaster, D.M. and Kushlan, D.M. (1996) *J. Am. Chem. Soc.*, **118**, 9255–9264.

Liou, Y.-C., Daley, M.E., Graham, L.A., Kay, C.M., Walker, V.K., Sykes, B.D. and Davies, P.L. (2000) *Protein Expr. Purif.*, **19**, 148–157.

Lipari, G. and Szabo, A. (1980) *J. Biophys.*, **30**, 489–506.

Lipari, G. and Szabo, A. (1981) *J. Chem. Phys.*, **75**, 2971–2976.

Lipari, G. and Szabo, A. (1982a) *J. Am. Chem. Soc.*, **104**, 4546–4559.

Lipari, G. and Szabo, A. (1982b) *J. Am. Chem. Soc.*, **104**, 4559–4570.

London, R.E. (1980) In *Magnetic Resonance in Biology*, Cohen, J.S. (Ed.), Vol. 1, Wiley, New York, pp. 1–69.

London, R.E. and Avitabile, J. (1978) *J. Am. Chem. Soc*., **100**, 7159–7165.

Marshall, C.B., Daley, M.E., Graham, L.A., Sykes, B.D. and Davies, P.L. (2002) *FEBS Lett.*, **529**, 261–267.

Mispelter, J., Lefevre, C., Adjadj, E., Quiniou, E. and Favaudon, V. (1995) *J. Biomol. NMR*, **5**, 233–244.

Muhandiram, R., Yamazaki, T., Sykes, B.D. and Kay, L.E. (1995) *J. Am. Chem. Soc.*, **117**, 11536–11544.

Nirmala, N.R. and Wagner, G. (1988) *J. Am. Chem. Soc.*, **110**, 7557–7558.

Palmer, A.G., Rance, M. and Wright, P.E. (1991a) *J. Am. Chem. Soc.*, **113**, 4371–4380.

Palmer, A.G., Wright, P.E. and Rance, M. (1991b) *Chem. Phys. Lett.*, **185**, 41–46.

Sklenar, V., Torchia, D. and Bax, A. (1987) *J. Magn. Reson.*, **73**, 375–379.

Tjandra, N., Feller, S.E., Pastor, R.W. and Bax, A. (1995) *J. Am. Chem. Soc.*, **117**, 12562–12566.

Tjandra, N., Wingfield, P., Stahl, S. and Bax, A. (1996) *J. Biomol. NMR*, **8**, 273–284.

Wand, A.J., Urbauer, J.L., McEvoy, R.P. and Bieber, R.J. (1996) *Biochemistry*, **35**, 6116–6125.

Wittebort, R.J. and Szabo, A. (1978) *J. Chem. Phys.*, **69**, 1722–1736.

Wolfram, S. (2002) *Mathematica 4.2*, Wolfram Research Inc. (http://www.wolfram.com)

Yamazaki, T., Muhandiram, R. and Kay, L.E. (1994) *J. Am. Chem. Soc.*, **116**, 8266–8278.

Yang, D., Mittermaier, A., Mok, Y.K. and Kay, L.E. (1998) *J. Mol. Biol.*, **276**, 939–954.